

INFLUENCE OF MONTMORILLONITE NANOCLAY CONTENT ON THE OPTICAL, THERMAL, MECHANICAL, AND BARRIER PROPERTIES OF LOW-DENSITY POLYETHYLENE

NATTINEE BUMBUDSANPHAROKE¹, WOOSEOK LEE¹, JAE CHUN CHOI², SE-JONG PARK², MEEKYUNG KIM², AND SEONGHYUK KO¹

¹ Department of Packaging, Yonsei University, 1 Yonseidae-gil, Wonju-si, Gangwon-do 26493, Republic of Korea

² Food Additives and Packaging Division, National Institute of Food and Drug Safety Evaluation, 187 Osongsaengmyeong 2-ro, Osong, Chungcheongbuk-do 28159, Republic of Korea

Abstract—Although low density polyethylene (LDPE) has long been widely used in packaging applications, some limitations in its use still exist and are due to its relatively poor gas barrier properties and low mechanical strength which can restrict its extensive use for more advanced applications, such as electronic and pharmaceutical packaging. The purpose of this study was to investigate the possibility of using montmorillonite (MMT) nanoclay as a means to enhance the thermal, mechanical, and barrier properties of LDPE prepared *via* melt extrusion. The level of exfoliated dispersion of the MMT nanoclay in the prepared LDPE-MMT composite was confirmed using transmission electron microscopy (TEM). The relationship between the resulting morphology and the thermal, mechanical, and barrier properties as a function of the MMT content was evaluated. The results showed that incorporating >3 wt.% of MMT nanoclay produced significant changes in the morphology of the LDPE-MMT nanoclay composite in that the segregated matrix adopted an oriented arrangement of exfoliated clay platelets. Thermogravimetric analysis (TGA) showed that the thermal stability of LDPE improved significantly as a result of MMT nanoclay incorporation. Furthermore, differential scanning calorimetry (DSC) analysis indicated that increasing clay content above 3 wt.% effectively reduces the crystallinity of LDPE-MMT composites through the suppression effect. The tensile strength of LDPE increased gradually with an increased content of MMT nanoclay and the maximum value of 16.89 N/mm² was obtained at 10 wt.% MMT content. This value represents a 40.87% increase relative to the tensile strength of the pristine LDPE. Barrier properties of LDPE and LDPE-MMT nanoclay composites were assessed by examining the permeability with respect to oxygen and water vapor. As the content of MMT nanoclay was increased to 10 wt.%, the permeability of the nanocomposite films to oxygen and water vapor notably decreased to 42.8% and 26.2%, respectively.

Key Words—Barrier Property, Food Packaging, Low-density, Mechanical, Montmorillonite Nanoclay, Optical, Thermal.

INTRODUCTION

Clay is a naturally occurring material that is primarily composed of fine-grained minerals that exhibit plasticity at certain water levels, but maintain the capacity to adopt a hardened state when dried or fired. Chemically, clay minerals are crystalline phyllosilicate minerals and essentially consist of hydrous Al silicates and occasionally hydrous Mg silicates. The clay minerals can also contain minor quantities of other elements, including K, Na, Ca, or Fe (Grim, 1942; Guggenheim and Martin, 1995). The variable properties and applications of clay minerals depend on the magnitude of the net negative layer charge that arises due to atomic substitutions, the layer type, the character of the tetrahedral and octahedral sheets, and the nature of the interlayer material (Hillier, 2003). Recently, layered silicates (*e.g.*, kaolinite, montmorillonite, mica, talc, vermiculite, saponite, and hectorite) have received significant attention in various

fields of research, such as agriculture, architecture, engineering, and materials science, because of potential applications as composites in rubber, ceramics, paper, polymers, and metal materials (Grim, 1942; Nair *et al.*, 1982; Zanetti *et al.*, 2000; Uddin, 2008).

Layered silicates have a characteristic platelet form, flaky soft structure, low specific gravity, and high aspect-ratio with a nano-scale thickness (Ganguly *et al.*, 2011). Different kinds of clay minerals are incorporated into polymers to improve their various characteristics, and most efforts by academic and industrial researchers in the packaging area have focused on montmorillonite (MMT) (Golebiewski *et al.*, 2008; Farhoodi, 2016). In nature, MMT is the major component in many bentonites and has a hydrophilic surface and MMT is only miscible with hydrophilic polymers (*i.e.* polyvinyl alcohol and polylactic acid). Most food packaging, however, is produced from petroleum based polymers which are hydrophobic (*i.e.* polyethylene and

* E-mail address of corresponding author:

s.ko@yonsei.ac.kr

DOI: 10.1346/CCMN.2017.064071

This paper was originally presented during the 3rd Asian Clay Conference, November 2016, in Guangzhou, China.

polypropylene). To improve the compatibility of MMT with an organophilic host matrix, the hydrophilic silicate surface (typically with Na^+ , K^+ , and Ca^+ as the exchanged cation) of clay minerals must be chemically modified with organic cations (*i.e.* alkylammonium salts) through ion-exchange reactions to yield an organophilic surface (Majeed *et al.*, 2013). The organic cation modification can decrease both the surface tension and wettability, and thereby result in an organophilic nanoclay that is compatible with the majority of thermoplastics (Golebiewski *et al.*, 2008). Due to these properties, the use of ultrafine, dispersed clay nanoparticles as fillers or additives offers new technological and economic opportunities for various applications (Zenetti *et al.*, 2000; Uddin, 2008; Gul *et al.*, 2016). The field of nanotechnology, especially the hybrid materials based on organic polymers and inorganic clay minerals with MMT, has come to the attention of many academic and industrial researchers. The addition of a small amount of a well dispersed MMT nanoclay (<10 wt.%) can substantially enhance the properties of pristine polymers (Albdiry *et al.*, 2013). Generally, MMT nanoclays do not easily disperse in polymers due to the preferred face-to-face stacking of agglomerated tactoids. Once an exfoliated state is achieved, however, a polymer matrix can exhibit significantly improved properties, especially increased modulus, thermal stability, flame retardancy, gas and water vapor barrier properties, and decreased solvent uptake (LeBaron *et al.*, 1999; Pavlidou and Papispyrides, 2008). In this regard, numerous MMT nanoclay composites have been intensively developed using various commodity polymers, such as polyethylene (Deka and Maji, 2010; Sadeghipour *et al.*, 2013; Majeed *et al.*, 2014; Scarfato *et al.*, 2016; Sepet *et al.*, 2016), polypropylene (Ataefard and Moradian, 2011b; Ataefard and Moradian, 2011a; Ragasamy *et al.*, 2011; Venkatesh *et al.*, 2012), polyethylene terephthalate (Kim *et al.*, 2013; Majdzaheh-Ardakani *et al.*, Meri *et al.*, 2014), polystyrene (Arora *et al.*, 2011; Paul *et al.*, 2013; Akbari and Bagheri, 2014), and polyamide (Agarwal *et al.*, 2014; Vyas and Iroh, 2014; Follain *et al.*, 2016).

Among the commodity plastics used in the packaging industries, LDPE is the simplest and the most widely used for food packaging applications with various formats, *i.e.*, films, sheets, bottles, cups, tubes, and trays (Marsh and Bugusu, 2007; Verghese *et al.*, 2012; Bodaghi *et al.*, 2015) due to the good heat-sealability, chemical inertness, and safety of LDPE as a food contact material. Conventional LDPE is a good–moderate moisture barrier, but has a low tensile strength and has poor gas barrier properties against oxygen and carbon dioxide (Driscoll and Paterson, 1999; Ractanapun and Ractanapun, 2011). Various efforts have been made to improve the fundamental properties of LDPE for use in active food packaging as an advanced functional material. A large number of hybrid systems have been

investigated by blending organic or inorganic particles (*i.e.* silica, calcium carbonate, graphene, silver nanoparticles, *etc.*) into a LDPE matrix to enhance the modulus strength and gas barrier properties (Arunvisut *et al.*, 2007; Zhong *et al.*, 2007; Wang *et al.*, 2011; Huang *et al.*, 2015; Lange *et al.*, 2015; Bumbudsanpharoke *et al.*, 2017).

The present study aimed to comprehensively study the influence of an exfoliated MMT nanoclay incorporated into LDPE and, in particular, the effect of various amounts of MMT on the morphological, optical, thermal, mechanical, and barrier characteristics of the LDPE–MMT nanoclay composites that result. The crystallinity and the MMT nanoclay distribution in the LDPE matrix were also to be examined.

MATERIALS AND METHODS

Materials

The Lutem LB7500 LDPE (LG Chemical Co., Yeosu, South Jeolla, Korea) with a melt flow index (MFI) of 7.5 g/10 min (ASTM D1238) and a density of 0.918 g/cm³ was employed in this study. The NanoMax[®]-LDPE, which contains 50 wt.% Nanomer[®] I.44P MMT nanoclay (Nanocor Inc., Hoffman Estates, Illinois, USA) was used as the masterbatch. The Nanomer I.44P is an onium ion modified MMT clay that contains 60% clay (CAS No. 1318-93-0) and 40% dimethyl dialkyl (C_{14} – C_{18}) ammonium organic modifier (CAS no. 61789-80-8).

Preparation of LDPE–MMT nanoclay composite films

The LDPE–MMT nanoclay composite films were prepared by melt-extrusion to yield composite film samples with MMT nanoclay contents of 0, 0.5, 1, 3, 5, and 10 wt.%. The composite films were processed using a laboratory-scale, twin-screw extruder (BA-19, BauTek Co., Pocheon, Gyeonggi, Korea) with a length/diameter (L/D) ratio of 40:19. The LDPE and MMT nanoclay masterbatch pellets were dried in a convection oven at 80°C for 24 h and mixed in a sealed plastic bag by manual tumbling prior to being fed into the extruder. The temperatures for the eight different processing zones from the feeder to the horizontal header of the extruder were set at 110, 110, 180, 190, 185, 180, 175, and 170°C and the screw speed rate was maintained at 300 rpm. The composite films were maintained at a thickness of approximately 60 μm in order to facilitate evaluation of the physical properties.

Characterization of LDPE–MMT nanoclay composite films

X-ray diffraction patterns were obtained using a Bruker D2 Phaser X-ray diffractometer (Bruker, Billerica, Massachusetts, USA) with Ni-filtered $\text{Cu K}\alpha$ radiation ($\lambda = 1.5406 \text{ \AA}$). Fourier-transform infrared (FTIR) spectra were recorded with a PerkinElmer

Spectrum 65 spectrophotometer (PerkinElmer Co. Ltd., Waltham, Massachusetts, USA) in attenuated total reflection (ATR) mode with a C/ZnSe crystal. Each spectrum was obtained in transmittance mode with sixteen scans and a resolution of 2 cm^{-1} in the wavenumber range of $400\text{--}4000\text{ cm}^{-1}$.

The surface morphology and cross section of each of the prepared composite sheets were observed using a Quanta FEG 250 field-emission scanning electron microscope (FE-SEM) (FEI Ltd., Hillsboro, Oregon, USA). Prior to analysis, the specimens were sputter coated with Pt/Pd using a Cressington Sputter Coater 108 auto (Cressington Scientific Instruments, Chalk Hill, Watford, UK). Further elemental analyses were performed using an Ametek energy-dispersive X-ray spectrometer (EDS) (Ametek, Berwyn, Pennsylvania, USA) attached to the FE-SEM. The shape and size of impregnated MMT nanoclays were examined using a Tecnai G2 Spirit Twin transmission electron microscope (TEM) (FEI Ltd., Hillsboro, Oregon, USA) operated at 120 kV. Each sample was embedded in Struers Caldofix resin (Columbus Chemical Industries, Columbus, Wisconsin, USA) and the resulting blocks were cryo-ultrathin sectioned at -80°C to a thickness of 80 nm using an EM FC7 Ultramicrotome (Leica, Nussloch, Germany) to produce cross sections of the composite films. Each prepared ultrathin section was transferred onto a 200-mesh C-coated Cu grid prior to TEM analysis.

Optical properties of the MMT nanoclay composite films were characterized with respect to CIE $L^*a^*b^*$ color values and transparency. The CIE $L^*a^*b^*$ values were measured using a CR-10 handheld color reader (Konica Minolta, Tokyo, Japan) and were recorded in triplicate for each sample. The opacity of the films was determined using a V-600 spectrophotometer (Jasco, Tokyo, Japan). The absorbance spectra of the films were recorded in the $200\text{--}800\text{ nm}$ range. The opacity of films was calculated using equation 1:

$$\text{Opacity} = \frac{Abs_{600}}{X} \quad (1)$$

where Abs_{600} is the absorbance value at 600 nm and X is the film thickness (mm).

Thermogravimetric analysis (TGA) was performed using a TGA 4000 thermogravimetric analyzer (PerkinElmer Co. Ltd., Waltham, Massachusetts, USA). The samples were heated from 30°C to 800°C at a rate of $10^\circ\text{C}/\text{min}$ under a flow of N_2 (20 mL/min).

A non-isothermal crystallization study was performed using a Q20 differential scanning calorimetry (DSC) instrument (TA Instruments, Castle, Delaware, USA). About 5–6 mg of each sample was accurately weighed and encapsulated in an Al pan. An empty sealed Al pan was used as a reference. All DSC tests were conducted under a N_2 atmosphere. The samples were heated at a constant rate of $10^\circ\text{C}/\text{min}$ from 30°C to 250°C (the first

heating scan) and held at this temperature for five minutes to erase the thermal and morphological history and to permit complete melting of any crystals present. Subsequently, the samples were cooled to -60°C at a constant rate of $-10^\circ\text{C}/\text{min}$ (cooling scan) in order to study the crystallization behavior. Finally, the samples were heated again for the second time (the second heating scan) at a rate of $10^\circ\text{C}/\text{min}$ to 250°C to melt the crystals that formed during the cooling procedure and to determine the melting temperature of each sample. All DSC curves were normalized to the unit weight of the sample.

Measurements of the tensile strength and elongation at break of as-prepared LDPE-MMT nanoclay composite films were performed according to ASTM D882–02 (ASTM D882-02, 2002) using a DTU-900MHA tensile tester (Daekyung Tech Co., Incheon, Korea) which employed a load cell with 10 kg force. Dumbbell-shaped test specimens were die cut to 5 mm width and 10 mm length (test region) and conditioned at 50% relative humidity (RH) and 23°C for 48 h prior to the measurements. Each specimen was stretched at a constant crosshead speed of 10 mm/min. Ten replicates were performed for each composite film and the average value was reported.

The oxygen transmission rates (OTR) of the LDPE-MMT nanoclay composite films were measured using an OTR 8001 oxygen permeation analyzer (Systech Instruments Co. Ltd., Johnsburg, Illinois, USA) at 23°C and 0% RH according to the ASTM D3985 method. The OTR results were normalized with respect to the film thickness to yield the oxygen permeability. The values obtained for each sample over three runs were averaged and reported.

The water vapor transmission rate (WVTR) was determined using a WVTR 7001 water vapor permeation analyzer (Systech Instruments Co. Ltd., Johnsburg, Illinois, USA) at 38°C and 95% RH according to the ASTM F1249 method. The area of the test films was 50 cm^2 . The WVTR results were normalized with respect to the film thickness to yield the water vapor permeabilities. The values obtained for each sample over three runs were averaged and reported.

Statistical analysis

Statistical comparisons were carried out using the SPSS[®] program (SPSS Inc., Chicago, Illinois, USA). The results were first interpreted using the one-way analysis of variance (ANOVA) with a confidence level of 95% ($\alpha = 0.05$), followed by analysis using Duncan's post-hoc test method (Morgan and Greigo, 1998). Data were represented in the form of a mean \pm standard deviation (SD). A p-value (probability value) was used to determine significant differences between the samples. A p-value of less than 0.05 indicates that the mean values of the compared specimens are significantly different.

RESULTS AND DISCUSSION

The XRD patterns of pristine LDPE and LDPE-MMT nanoclay composites had significant increases in the intensities of the 6 and 18°2 θ diffraction peaks observed for samples with 0.5 wt.% nanoclay (Figure 1). These peaks were assigned to the (001) and (020) planes of the clay stacked-layer structure and agreed with values reported by Zbik and Frost (2010) and Pujala (2014). At low volume fractions of the MMT nanoclay, these diffraction peaks appeared as very weak shoulders. As the content of MMT nanoclay was increased, however, the same peaks became significantly more pronounced.

FTIR is widely used for the identification of specific chemical groups in materials. Clear additional absorption peaks were identified at about 464, 521, and 1047 cm^{-1} (highlighted with black arrows in Figure 2) in the FTIR spectra of MMT nanoclay composite films. These values correspond to IR absorption peaks typical for silica and alumina and most likely originated from the stretching and bending modes (Zazoum *et al.*, 2013). The peaks characteristic of the MMT nanoclay became more intense as the content of MMT nanoclay in the composite system was increased.

The morphology of LDPE-MMT nanoclay composite films was observed using FE-SEM (Figure 3). The cross-sectional surface of the pristine LDPE displayed a continuous phase without any voids. In contrast, the surface of films that contained higher contents of MMT nanoclay showed micro-voids and segregated structures (labeled with yellow arrows, white grayscale), which were thought to arise due to the dispersion of MMT nanoclay in LDPE. The oriented arrangement of clay platelets was absent in composites prepared using <3 wt.% of clay, which implies that the MMT nanoclays were homogeneously embedded in the LDPE matrix. On the other hand, when the MMT nanoclay concentration

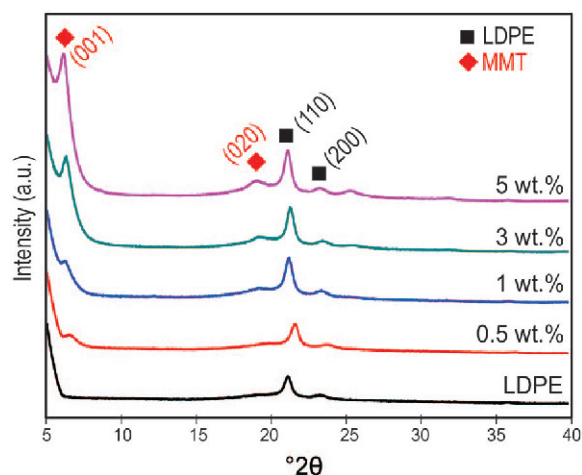


Figure 1. XRD patterns of LDPE and LDPE-MMT nanoclay composites.

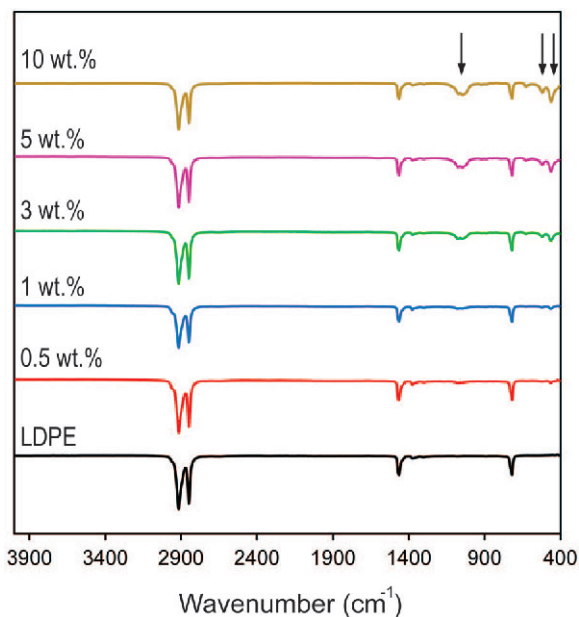


Figure 2. FTIR spectra of LDPE and LDPE-MMT nanoclay composites. The arrows shown at frequencies of 464, 521, and 1,047 cm^{-1} indicate the presence of the MMT nanoclay as the stretching and bending modes of silica and alumina.

exceeded 3 wt.%, the formation of sheet-like layered structures laid parallel to the film surface was observed. This arrangement was most likely initiated by and along the direction of the shear flow during the extrusion and film forming processes as reported by Chen *et al.* (2000) and Morgan and Gilman (2003).

The MMT nanoclay particles dispersed in the LDPE matrix can be readily identified using TEM as dark lines in the LDPE-MMT composite film that was prepared using 5 wt.% nanoclay (Figure 4a). The TEM analysis revealed that a large proportion of the clay layers was in the exfoliated state. Lan (2012) and Panwar *et al.* (2011) reported that the shear force exerted during the extrusion process promoted nanoparticle dispersion by partially disrupting the stacking order of clay layers, while the molten polymer can at the same time enter and penetrate the MMT nanoclay interlayers. Close examination of some platelets (highlighted with yellow arrows in Figure 4b, white grayscale), however, revealed the presence of stacked structures, which suggests that some intercalated features in the LDPE matrix remain. Siengchin (2011) explained that the shear force exerted by the extrusion process is not always sufficiently high to achieve complete break-up of large agglomerates, which thereby allows clusters of nanoparticles to persist. Put together, these results indicate that the clay layers in LDPE-MMT nanocomposite films were present in a mixed form and mostly consisted of well dispersed exfoliated layers with a small amount of intercalated MMT nanoclays.

The digital images of pristine LDPE and LDPE-MMT nanoclay films were taken for optical comparison

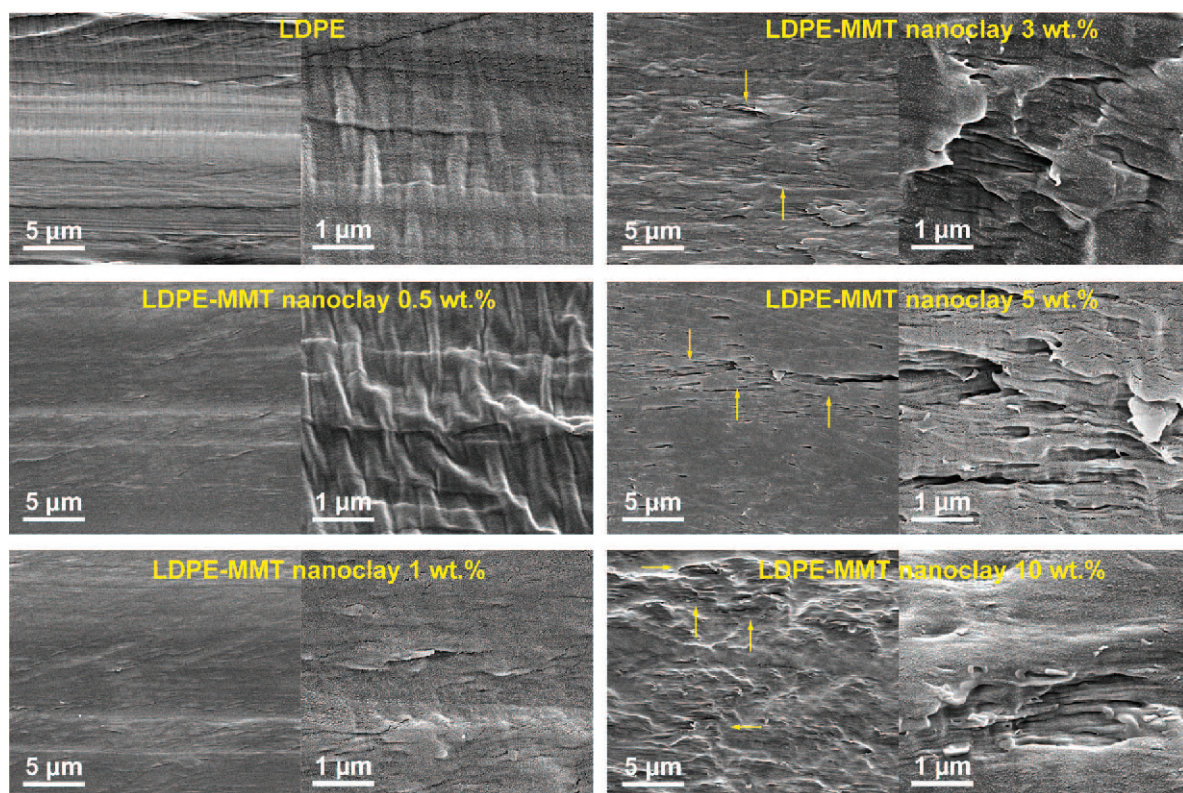


Figure 3. FE-SEM cross-sectional micrographs of LDPE and LDPE-MMT nanoclay composites.

(Table 1). These images showed that the originally transparent LDPE film gained a slightly yellowish tint when MMT nanoclay particles were added. In order to

investigate the origin of these color differences, the values of L^* , a^* , and b^* were measured for all prepared samples (Table 1). The incorporation of MMT nanoclay

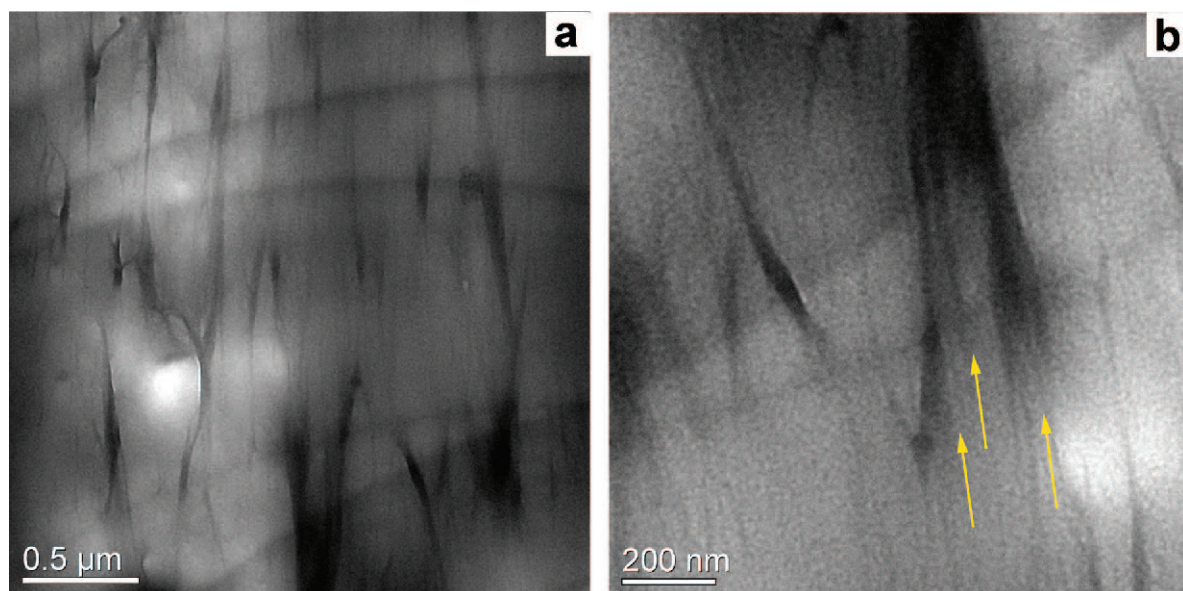








Figure 4. TEM micrographs of an intercalated LDPE–MMT nanoclay composite with different scales (a) 0.5 μm and (b) 200 nm. Arrows indicate the presence of intercalated MMT nanoclays in the LDPE matrix.

Table 1. Effect of MMT nanoclay content on the color and opacity of LDPE-MMT nanoclay composite films with pristine LDPE values provided for comparison.

Sample	Digital Photo	L*	a*	b*	Abs. @600 nm	Opacity (a.u./mm)
LDPE		56.8 ± 0.10 ^a	10.13 ± 0.06 ^{ac}	7.9 ± 0.00 ^a	0.0430	0.717
LDPE-MMT nanoclay 0.5 wt.%		56.8 ± 0.00 ^a	10.06 ± 0.06 ^b	8.0 ± 0.05 ^a	0.0435	0.725
LDPE-MMT nanoclay 1 wt.%		56.7 ± 0.12 ^a	10.0 ± 0.00 ^{cb}	8.1 ± 0.06 ^b	0.0443	0.738
LDPE-MMT nanoclay 3 wt.%		56.4 ± 0.12 ^b	10.13 ± 0.06 ^{ac}	8.7 ± 0.05 ^c	0.0462	0.770
LDPE-MMT nanoclay 5 wt.%		56.1 ± 0.12 ^c	10.20 ± 0.10 ^c	9.1 ± 0.06 ^d	0.0478	0.797
LDPE-MMT nanoclay 10 wt.%		55.8 ± 0.10 ^d	10.30 ± 0.06 ^d	9.6 ± 0.06 ^c	0.0488	0.813

The color and opacity results are expressed in the form of a mean ± SD for n = 3. According to the Duncan's multiple range test statistical analysis, the values in the same column that are followed by a different letter are significantly different (p < 0.05).

into the LDPE film clearly affected the values of L* (lightness/darkness), a* (redness/greenness), and b* (yellowness/blueness) of the composite films. As reported in the literature (Landry *et al.*, 2010), however, the differences in color were only perceivable to the naked eye when the L*, a*, and b* parameter differences were >2. The results showed a statistically significant difference (P<0.05) in the value of b*, which increased from 7.9 ± 0.00 to 9.6 ± 0.006 as the MMT nanoclay concentration was increased from 0 to 10 wt.%. This b* value difference accounts for the yellow color that can be observed by the naked eye. In contrast to b*, the values of L* and a* exhibited only very small changes when the MMT nanoclay loading was altered. Opacity

can be determined by measuring the transparency of a film. A material is generally considered to be opaque when it absorbs and/or reflects light, but does not transmit it. A higher value for opacity, therefore, is typically associated with lower transparency (Villarreal *et al.*, 2011). The opacity in the prepared samples was evaluated by measuring absorbance at a wavelength of 600 nm using a UV-Vis spectrophotometer (Table 1). The opacity values of the nanocomposite films tended to increase as the content of MMT nanoclay increased. Shojaee-Aliabadi *et al.* (2014) suggested that the main reason for the loss of transparency in composite films was a result of the incorporation of increasingly high contents of clay. This can be attributed to the aggrega-

Table 2. Melting temperature, melting enthalpy, and crystallinity values for 10% and 50% weight loss determined using DSC for LDPE and LDPE-MMT nanoclay composite films.

Sample	Temperature at 10% weight loss (°C)	Temperature at 50% weight loss (°C)	T_m (°C)	Melting Enthalpy (J/g)	Crystallinity (%)
LDPE	437	476	107.01	161.0	54.95
LDPE-MMT nanoclay 0.5 wt.%	450	484	105.87	170.0	58.02
LDPE-MMT nanoclay 1 wt.%	450	486	105.98	179.0	61.09
DPE-MMT nanoclay 3 wt.%	461	491	106.42	180.5	61.60
LDPE-MMT nanoclay 5 wt.%	464	493	106.11	162.0	55.29
LDPE-MMT nanoclay 10 wt.%	465	496	106.21	161.9	55.26

tion of nanoparticles, which obstructed the transmission of light (Guo *et al.*, 2013).

The thermal degradation behavior of a polymer in terms of weight loss as a function of temperature is typically determined using TGA. The important parameters in such analyses are the degradation onset temperature ($T_{10\%}$, determined as the point at which 10% of the sample weight has been lost) and the degradation mid-point ($T_{50\%}$) (Olewnik *et al.*, 2010). In the present study, the thermal stability of nanocomposites was generally higher in comparison to the pristine LDPE (Table 2). The temperature marking the onset of thermal degradation ($T_{10\%}$) was significantly higher in the nanocomposites than that determined for LDPE (437°C). The $T_{50\%}$ value of the nanocomposites was also found to increase with increasing MMT nanoclay content and the maximum $T_{50\%}$ value of 496°C was determined at 10 wt.% MMT nanoclay loading. These results are in agreement with those reported in other studies (Olewnik *et al.*, 2010; Silva *et al.*, 2014). These improvements in thermal stability can be explained by the formation of an insulating and incombustible multi-layered carbonaceous–silicate char on the composite surface during combustion. This char can obstruct the escape and diffusion of low molecular weight volatile products within the nanocomposites, while simultaneously insulating the polymer underneath the char layer from surrounding heat (Modesti *et al.*, 2006; Olewnik *et al.*, 2010; Hemati and Garmabi, 2011). The physical-chemical adsorption of volatile decomposition products on silicates/clays, additionally, can delay the volatilization of products that are generated from carbon-carbon bond scission within the LDPE matrix (Chafidz *et al.*, 2014).

The thermal properties of LDPE-MMT nanoclay composites, such as melting temperature, fusion

enthalpy, and degree of crystallinity for non-isothermal crystallization, were also studied using DSC. The degree of crystallinity was calculated according to the following equation:

$$X_C = \frac{\Delta H_m}{\Delta H_m^0} \times 100 \quad (2)$$

where ΔH_m is the experimental heat of fusion (J/g) and ΔH_m^0 is the theoretical heat of fusion of 100% crystalline LDPE (293J/g) (Wunderlich and Czornyj, 1977). The melting temperature (T_m) and the heat of fusion were determined during the second round of heating and are shown for each sample in Table 2.

The DSC analysis showed that the melting temperature (T_m) decreased slightly as the MMT nanoclay content was increased. This change can be attributed to the differences in crystal properties (*e.g.*, crystal type, packing density, crystallite size, and distribution) between the nanocomposites and pristine LDPE (Qi *et al.*, 2006; Sorrentino *et al.*, 2007; Olewnik *et al.*, 2010). A study by Monica *et al.* (2014) revealed that layers of MMT nanoclay can act as nucleating agents that facilitate crystal growth by providing a higher level of nucleation density (Olewnik *et al.*, 2010). This process may involve crystal formation and accounts for the changes in T_m . In addition, an increase in the clay mineral content to 3 wt.% increased significantly both the melting enthalpy and crystallinity. Specifically, a 12% increase in crystallinity for the nanocomposites was observed, which suggests that the filler in the LDPE matrix played a role in nucleation processes (Olewnik *et al.*, 2010). Monica *et al.* (2014) reported that the crystallinity of LDPE/PE-g-MA/clay composite (where PE-g-MA represents polyethylene grafted maleic anhydride) increased with an increased content of organo-

montmorillonite and that the maximum of crystallinity was found at 3 wt.% clay mineral content. The authors additionally found that the level of crystallinity decreased with a further increase in clay mineral content. This observation is in agreement with the present results, which showed that the degree of crystallinity decreased when the MMT nanoclay concentration was increased above 3 wt.%. This behavior can be most likely explained by the “suppression effect” of clay particles at high content, as suggested by Homminga *et al.* (2006) and Mudaliar *et al.* (2006). Particularly, this behavior arose because the perfection of the crystals was affected by the restricted mobility of LDPE chain segments, which consequently slowed down the growth of well-developed lamellar crystals. This restriction increased with an increased content of MMT nanoclay and, thereby, yielded less perfect crystals. The combined influences of excess nucleation sites and retarded crystal growth led to the production of fine crystals, which, in turn, resulted in a lower degree of crystallinity (Di Maio *et al.*, 2004; Kontou and Niaounakis, 2006; Mudaliar *et al.*, 2006; Zazoum *et al.*, 2014; Chen *et al.*, 2015).

The tensile strength and elongation were examined as a function of clay mineral content (Figure 5). The results revealed that the tensile strength in the machine direction increased significantly from 11.99 N/mm² to 16.89 N/mm² as the clay mineral content was increased from 0 wt.% to 10 wt.%. This result revealed two possible explanations for the increase in tensile strength in the prepared LDPE-MMT nanoclay composites. The first explanation may stem from an increase in crystallinity as was observed in the DSC analyses. The greater the crystallinity, the greater the energy absorbed and the greater the modulus (Tanniru *et al.*, 2006; Santos *et al.*, 2013). Although the mechanical properties of a nanocomposite are related to the crystallinity of the polymer matrix, Tanniru *et al.* (2006) observed that the behavior

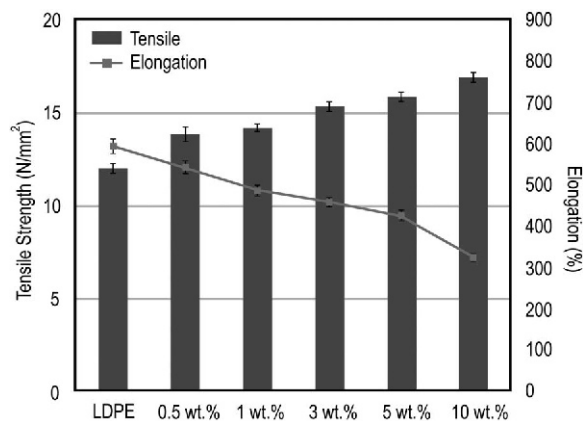


Figure 5. Tensile strength and elongation in machine direction determined for LDPE and LDPE-MMT nanoclay composite films prepared using different clay contents.

of the composite was not simply a function of crystallinity and crystal structure (morphology), but was instead a complex function that involved additional factors, such as lamellar thickness and interfacial interactions. A comprehensive study by Ray (2013) showed that a filler with an aspect ratio greater than 20–30 can be considered as an effective reinforcement filler and yields a nanocomposite with apparently increased stiffness. The proposal from the present study was, therefore, that the improved tensile strength can be attributed to the high specific surface area (~750–800 m²/g) and large aspect ratio (~50–1000) of the well-dispersed MMT clay within the LDPE matrix (Nasiri *et al.*, 2016). Similarly, previous work has shown that the dispersion of nano-scale silicate layers in a polyolefin matrix led to an improvement in mechanical strength (Liu and Wu, 2001; Arunvisut *et al.*, 2007). The stiffness of MMT nanoclay plates hindered the mobility of polymer phases and prevented the slippage of polymer chains past one another. The stiffness also retarded the plastic deformation and, thereby, resulted in stretching resistance and lower elongation (Noh and Lee, 1999; Liu and Wu, 2001; Azizi *et al.*, 2010). This description was supported by the decreased elongation of LDPE-MMT nanoclay composites as a function of increased clay mineral content (Figure 5). The elongation dropped significantly from 592.28% for pristine LDPE to about 323.50% for the LDPE-MMT with 10 wt.% clay mineral content. Chen *et al.* (2003) and Fu and Naguib (2006) proposed that this reduction stemmed from the weak interactions between the polymer matrix and fillers as well as from the formation of agglomerated nanoclay, which created stress concentrations in the polymer matrix. LDPE, therefore, lost its plastic properties as a result of the increased stiffness value.

The LDPE-MMT nanoclay composites showed similar trends in behavior for both the oxygen and water vapor permeability (Figure 6). The permeability was found to decrease gradually as the concentration of clay mineral increased from 0.5 wt.% to 10 wt.%.

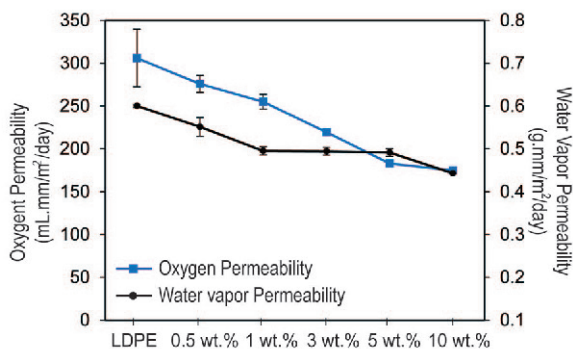


Figure 6. Oxygen and water-vapor permeability values of LDPE and LDPE-MMT nanoclay composite films prepared using different clay contents.

Specifically, oxygen permeability decreased from 306 to 175 mL mm/m²day atm (42.8% reduction) while the water vapor permeability decreased from 0.600 to 0.443 g mm/m²day atm (26.2% reduction). These changes most likely arose as a result of the high aspect ratio of exfoliated and intercalated clay platelets in the LDPE matrix. In particular, as shown in Figure 3 and Figure 4, when the layers are aligned in the direction parallel to the film surface, the resulting tortuous path delays diffusion of both gas and water vapor (Arunvisut *et al.*, 2007; Decker *et al.*, 2015).

CONCLUSION

Herein, LDPE-MMT nanoclay composites with different MMT nanoclay loadings were prepared successfully using melt extrusion. TEM confirmed that MMT nanoclay was well dispersed in the LDPE matrix and exhibited exfoliation and partial intercalation. FE-SEM images revealed that the arrangement in LDPE-MMT nanoclay composites consists of sheet-like structures that are oriented parallel to the film surface. Owing to the formation of an insulating char layer during combustion, MMT nanoclay composites were found to be more thermally stable than pristine LDPE. The overall thermal stability was also found to increase with an increased content of MMT nanoclay. The results showed that the mid-point decomposition temperature ($T_{50\%}$) of the nanocomposite prepared with 10 wt.% MMT is 493°C, which is a value that is 20°C higher than that of pristine LDPE (476°C). The tensile strength of this nanocomposite improved clearly by 40.87% in comparison to that of the pristine LDPE. A significant decrease in oxygen permeability (42.8%) and water vapor permeability (26.2%) with an increased MMT nanoclay content of up to 10 wt.% was observed due to the tortuous structure across the LDPE matrix. Thus, as discussed above, the well-dispersed MMT nanoclay not only acted as thermal insulator and stress absorber, but also created a tortuous inner path in the LDPE matrix, and, thereby, promoted the thermal, mechanical, and barrier properties of LDPE. A warning, however, is that the excessive addition of nanoclay can cause morphological defects and lower crystallinity, which results in adverse effects on barrier and thermal stability.

ACKNOWLEDGMENTS

This research was supported by a grant (15162MFDS031) in 2015 from the Ministry of Food and Drug Safety, South Korea.

REFERENCES

Agarwal, A., Raheja, A., Natarajan, T.S., and Chandra, T.S. (2014) Effect of electrospun montmorillonite-nylon 6 nanofibrous membrane coated packaging on potato chips and bread. *Innovative Food Science & Emerging Technologies*, **26**, 424–430.

Akbari, B. and Bagheri, R. (2014) Influence of nanoclay on morphology, mechanical properties and deformation mechanism of polystyrene. *Polymer-Plastics Technology and Engineering*, **53**, 156–161.

Albdiry, M.T., Yousif, B.F., Ku, H., and Lau, K.T. (2013) A critical review on the manufacturing processes in relation to the properties of nanoclay/polymer composites. *Journal of Composite Materials*, **47**, 1093–1115.

Arora, A., Choudhary, V., and Sharma, D.K. (2011) Effect of clay content and clay/surfactant on the mechanical, thermal and barrier properties of polystyrene/organoclay nanocomposites. *Journal of Polymer Research*, **18**, 843–857.

Arunvisut, S., Phummanee, S., and Somwangthanaroj, A. (2007) Effect of clay on mechanical and gas barrier properties of blown film LDPE/clay nanocomposites. *Journal of Applied Polymer Science*, **106**, 2210–2217.

ASTM D882-02 (2002) *Standard Test Method for Tensile Properties of Thin Plastic Sheeting*. American Society for Testing and Materials, Philadelphia, USA.

Ataefard, M. and Moradian, S. (2011a) Polypropylene/organoclay nanocomposites: Effects of clay content on properties. *Polymer-Plastics Technology and Engineering*, **50**, 732–739.

Ataefard, M. and Moradian, S. (2011b) Surface properties of polypropylene/organoclay nanocomposites. *Applied Surface Science*, **257**, 2320–2326.

Azizi, H., Morshedani, J., Barikani, M., and Wagner, M.H. (2010) Effect of layered silicate nanoclay on the properties of silane crosslinked linear low-density polyethylene (LLDPE). *Express Polymer Letters*, **4**, 252–262.

Bodaghi, H., Mostofi, Y., Oromiehie, A., Ghanbarzadeh, B., and Hagh, Z.G. (2015) Synthesis of clay-TiO₂ nanocomposite thin films with barrier and photocatalytic properties for food packaging application. *Journal of Applied Polymer Science*, **132**, 41764(41761–41768).

Bumbudsanpharoke, N., Lee, W., and Ko, S. (2017) A comprehensive feasibility study on the properties of LDPE-Ag nanocomposites for food packaging applications. *Polymer Composites*, 1–9.

Chafidz, A., Kaavessina, M., Al-Zahrani, S., and Al-Otaibi, M.N. (2014) Polypropylene/organoclay nanocomposites prepared using a Laboratory Mixing Extruder (LME): Crystallization, thermal stability and dynamic mechanical properties. *Journal of Polymer Research*, **21**, 1–18.

Chen, G.M., Qi, Z.N., and Shen, D.Y. (2000) Shear-induced ordered structure in polystyrene/clay nanocomposite. *Journal of Materials Research*, **15**, 351–356.

Chen, J.B., Xu, J.Z., Xu, H., Li, Z.M., Zhong, G.J., and Lei, J. (2015) The crystallization behavior of biodegradable poly(*n*-butylene succinate) in the presence of organically modified clay with a wide range of loadings. *Chinese Journal of Polymer Science*, **33**, 576–586.

Chen, L., Wong, S.C., and Pisharath, S. (2003) Fracture properties of nanoclay-filled polypropylene. *Journal of Applied Polymer Science*, **88**, 3298–3305.

Decker, J.J., Meyers, K.P., Paul, D.R., Schiraldi, D.A., Hiltner, A., and Nazarenko, S. (2015) Polyethylene-based nanocomposites containing organoclay: A new approach to enhance gas barrier via multilayer coextrusion and interdiffusion. *Polymer*, **61**, 42–54.

Deka, B.K. and Maji, T.K. (2010) Effect of coupling agent and nanoclay on properties of HDPE, LDPE, PP, PVC blend and Phargamites karka nanocomposite. *Composites Science and Technology*, **70**, 1755–1761.

Di Maio, E., Iannace, S., Sorrentino, L., and Nicolais, L. (2004) Isothermal crystallization in PCL/clay nanocomposites investigated with thermal and rheometric methods. *Polymer*, **45**, 8893–8900.

Driscoll, R.H. and Paterson, J.L. (1999) Packaging and food

- preservation. Pp. 687 in: *Handbook of Food Preservation* (M.S. Rahman, editors). Marcel Dekker, New York.
- Farhoodi, M. (2016) Nanocomposite Materials for Food Packaging Applications: Characterization and Safety Evaluation. *Food Engineering Reviews*, **8**, 35–51.
- Follain, N., Alexandre, B., Chappey, C., Colasse, L., Mederic, P., and Marais, S. (2016) Barrier properties of polyamide 12/montmorillonite nanocomposites: Effect of clay structure and mixing conditions. *Composites Science and Technology*, **136**, 18–28.
- Fu, J. and Naguib, H.E. (2006) Effect of nanoclay on the mechanical properties of PMMA/clay nanocomposite foams. *Journal of Cellular Plastics*, **42**, 325–342.
- Ganguly, S., Dana, K., Mukhopadhyay, T.K., Parya, T., and Ghatak, S. (2011) Organophilic nano clay: A comprehensive review. *Transactions of the Indian Ceramic Society*, **70**, 189–206.
- Golebiewski, J., Rozanski, A., Dzwonkowski, J., and Galeski, A. (2008) Low density polyethylene–montmorillonite nanocomposites for film blowing. *European Polymer Journal*, **44**, 270–286.
- Grim, R.E. (1942) Modern concepts of clay materials. *The Journal of Geology*, **50**, 225–275.
- Guggenheim, S. and Martin, R. (1995) Definition of clay and clay mineral: Joint report of the AIPEA nomenclature and CMS nomenclature committees. *Clays and Clay Minerals*, **43**, 255–256.
- Gul, S., Kausar, A., Muhammad, B., and Jabeen, S. (2016) Research progress on properties and applications of polymer/clay nanocomposite. *Polymer-Plastics Technology and Engineering*, **55**, 684–703.
- Guo, J.M., Li, X.Y., Mu, C.D., Zhang, H.G., Qin, P., and Li, D.F. (2013) Freezing-thawing effects on the properties of dialdehyde carboxymethyl cellulose crosslinked gelatin-MMT composite films. *Food Hydrocolloids*, **33**, 273–279.
- Hemati, F. and Garmabi, H. (2011) Compatibilised LDPE/LLDPE/nanoclay nanocomposites: I. Structural, mechanical, and thermal properties. *The Canadian Journal of Chemical Engineering*, **89**, 187–196.
- Hillier, S. (2003) Clay Mineralogy. Pp. 139–142 in: *Encyclopaedia of Sediments and Sedimentary Rocks* (G.V. Middleton, M.J. Church, M. Coniglio, L.A. Hardie, F.J. Longstaffe, editors). Academic Publishers, Dordrecht, The Netherlands.
- Homminga, D.S., Goderis, B., Mathot, V.B.F., and Groeninckx, G. (2006) Crystallization behavior of polymer/montmorillonite nanocomposites. Part III. Polyamide-6/montmorillonite nanocomposites, influence of matrix molecular weight, and of montmorillonite type and concentration. *Polymer*, **47**, 1630–1639.
- Huang, H.D., Zhou, S.Y., Ren, P.G., Ji, X., and Li, Z.M. (2015) Improved mechanical and barrier properties of low-density polyethylene nanocomposite films by incorporating hydrophobic graphene oxide nanosheets. *RSC Advances*, **5**, 80739–80748.
- Kim, S.G., Lofgren, E.A., and Jabarin, S.A. (2013) Dispersion of nanoclays with poly(ethylene terephthalate) by melt blending and solid state polymerization. *Journal of Applied Polymer Science*, **127**, 2201–2212.
- Kontou, E. and Niaounakis, M. (2006) Thermo-mechanical properties of LLDPE/SiO₂ nanocomposites. *Polymer*, **47**, 1267–1280.
- Lan, T. (2012) Nanocomposites for food packaging: An overview. Pp. 406–413 in: *Bionanotechnology: A Revolution in Food, Biomedical and Health Sciences* (D. Bagchi, M. Bagchi, H. Moriyama, F. Shahidi, editors). John Wiley & Son, West Sussex, UK.
- Landry, V., Blanchet, P., and Riedl, B. (2010) Mechanical and optical properties of clay-based nanocomposites coatings for wood flooring. *Progress in Organic Coatings*, **67**, 381–388.
- Lange, S., Arroval, T., Saar, R., Kink, I., Aarik, J., and Krumme, A. (2015) Oxygen barrier properties of Al₂O₃- and TiO₂-coated LDPE films. *Polymer-Plastics Technology and Engineering*, **54**, 301–304.
- LeBaron, P.C., Wang, Z., and Pinnavaia, T.J. (1999) Polymer-layered silicate nanocomposites: An overview. *Applied Clay Science*, **15**, 11–29.
- Liu, X.H. and Wu, Q.J. (2001) PP/clay nanocomposites prepared by grafting-melt intercalation. *Polymer*, **42**, 10013–10019.
- Majdzadeh-Ardakani, K., Lofgren, E.A., and Jabarin, S.A. (2014) The effect of particle size distribution on the dispersion of nanoclays in poly(ethylene terephthalate)/clay nanocomposites. *Journal of Reinforced Plastics and Composites*, **33**, 358–368.
- Majeed, K., Hassan, A., and Abu Bakar, A. (2014) Influence of maleic anhydride-grafted polyethylene compatibiliser on the tensile, oxygen barrier and thermal properties of rice husk and nanoclay-filled low-density polyethylene composite films. *Journal of Plastic Film & Sheeting*, **30**, 120–140.
- Majeed, K., Jawaid, M., Hassan, A., Abu Bakar, A., Khalil, H.P.S.A., Salema, A.A., and Inuwa, I. (2013) Potential materials for food packaging from nanoclay/natural fibres filled hybrid composites. *Materials & Design*, **46**, 391–410.
- Marsh, K. and Bugusu, B. (2007) Food packaging - Roles, materials, and environmental issues. *Journal of Food Science*, **72**, R39–R55.
- Meri, R.M., Zicans, J., Maksimovs, R., Ivanova, T., Kalnins, M., Berzina, R., and Japins, G. (2014) Elasticity and long-term behavior of recycled polyethylene terephthalate (rPET)/montmorillonite (MMT) composites. *Composite Structures*, **111**, 453–458.
- Modesti, M., Lorenzetti, A., Bon, D., and Besco, S. (2006) Thermal behaviour of compatibilised polypropylene nanocomposite: Effect of processing conditions. *Polymer Degradation and Stability*, **91**, 672–680.
- Monica, A.P., Bernabé, L.R., Karla, A.G.M., Víctor, H.C.R., Miguel, M., Johanna, C., and Álvaro, M. (2014) Low density polyethylene (LDPE) nanocomposites with passive and active barrier properties. *Journal of the Chilean Chemical Society*, **59**, 2442–2446.
- Morgan, A.B. and Gilman, J.W. (2003) Characterization of polymer-layered silicate (clay) nanocomposites by transmission electron microscopy and X-ray diffraction: A comparative study. *Journal of Applied Polymer Science*, **87**, 1329–1338.
- Morgan, G.A. and Griego, O.V. (1998) *Easy Use and Interpretation of SPSS for Windows: Answering Research Questions with Statistics*. Lawrence Erlbaum Associates Inc., New Jersey, USA.
- Mudaliar, A., Yuan, Q., and Misra, R. (2006) On surface deformation of melt-intercalated polyethylene–clay nanocomposites during scratching. *Polymer Engineering & Science*, **46**, 1625–1634.
- Nair, R.R., Hashimi, N.H., and Rao, V.P. (1982) Distribution and dispersal of clay-minerals on the western continental-shelf of India. *Marine Geology*, **50**, M1–M9.
- Nasiri, A., Peyron, S., Gastaldi, E., and Gontard, N. (2016) Effect of nanoclay on the transfer properties of immanent additives in food packages. *Journal of Materials Science*, **51**, 9732–9748.
- Noh, M.W. and Lee, D.C. (1999) Synthesis and characterization of PS-clay nanocomposite by emulsion polymerization. *Polymer Bulletin*, **42**, 619–626.
- Olewnik, E., Garman, K., and Czerwinski, W. (2010) Thermal properties of new composites based on nanoclay, polyethylene and polypropylene. *Journal of Thermal Analysis and Calorimetry*, **101**, 323–329.

- Panwar, A., Choudhary, V., and Sharma, D.K. (2011) A review: Polystyrene/clay nanocomposites. *Journal of Reinforced Plastics and Composites*, **30**, 446–459.
- Paul, P., Hussain, S., Bhattacharjee, D., and Pal, M. (2013) Preparation of polystyrene–clay nanocomposite by solution intercalation technique. *Bulletin of Materials Science*, **36**, 361–366.
- Pavlidou, S. and Papaspyrides, C.D. (2008) A review on polymer–layered silicate nanocomposites. *Progress in Polymer Science*, **33**, 1119–1198.
- Pujala, R.K. (2014) *Dispersion Stability, Microstructure and Phase Transition of Anisotropic Nanodiscs*. Springer International Publishing, London.
- Qi, R.R., Jin, X., and Zhou, C.X. (2006) Preparation and properties of polyethylene–clay nanocomposites by an *in situ* graft method. *Journal of Applied Polymer Science*, **102**, 4921–4927.
- Rachtanapun, P. and Rachtanapun, C. (2011) Vacuum packaging. Pp. 861–874 in: *Handbook of Frozen Food Processing and Packaging 2nd edition* (D-W. Sun, editor). CRC Press, Florida, USA.
- Rangasamy, L., Shim, E., and Pourdeyhimi, B. (2011) Structure and tensile properties of nanoclay–polypropylene fibers produced by melt spinning. *Journal of Applied Polymer Science*, **121**, 410–419.
- Ray, S.S. (2013) *Clay-containing Polymer Nanocomposites: From Fundamentals to Real Applications*. Elsevier, Oxford, UK.
- Sadeghipour, H., Ebadi-Dehaghani, H., Ashouri, D., Mousavian, S., Hashemi-Fesharaki, M., and Gahrouei, M.S. (2013) Effects of modified and non-modified clay on the rheological behavior of high density polyethylene. *Composites Part B: Engineering*, **52**, 164–171.
- Santos, K.S., Demori, R., Mauler, R.S., Liberman, S.A., and Oviedo, M.A.S. (2013) The influence of screw configurations and feed mode on the dispersion of organoclay on PP. *Polimeros-Ciencia E Tecnologia*, **23**, 175–181.
- Scarfato, P., Incarnato, L., Di Maio, L., Dittrich, B., and Schartel, B. (2016) Influence of a novel organo-silylated clay on the morphology, thermal and burning behavior of low density polyethylene composites. *Composites Part B: Engineering*, **98**, 444–452.
- Sepet, H., Tarakcioglu, N., and Misra, R.D.K. (2016) Investigation of mechanical, thermal and surface properties of nanoclay/HDPE nanocomposites produced industrially by melt mixing approach. *Journal of Composite Materials*, **50**, 3105–3116.
- Shojaee-Aliabadi, S., Mohammadifar, M.A., Hosseini, H., Mohammadi, A., Ghasemlou, M., Hosseini, S.M., Haghshenas, M., and Khaksar, R. (2014) Characterization of nanobiocomposite kappa-carrageenan film with Zataria multiflora essential oil and nanoclay. *International Journal of Biological Macromolecules*, **69**, 282–289.
- Siengchin, S. (2011) Nano-scale reinforcing and toughening thermoplastics: Processing, structure and mechanical properties Pp. 215–240 in: *Nanofibers-Production, Properties and Functional Applications* (T. Lin, editor). InTech, Croatia.
- Silva, B.L., Nack, F.C., Lepienski, C.M., Coelho, L.A.F., and Becker, D. (2014) Influence of intercalation methods in properties of clay and carbon nanotube and high density polyethylene nanocomposites. *Materials Research*, **17**, 1628–1636.
- Sorrentino, A., Gorrasi, G., and Vittoria, V. (2007) Potential perspectives of bio-nanocomposites for food packaging applications. *Trends in Food Science & Technology*, **18**, 84–95.
- Tanniru, M., Yuan, Q., and Misra, R. (2006) On significant retention of impact strength in clay–reinforced high-density polyethylene (HDPE) nanocomposites. *Polymer*, **47**, 2133–2146.
- Uddin, F. (2008) Clays, nanoclays, and montmorillonite minerals. *Metallurgical and Materials Transactions A*, **39**, 2804–2814.
- Venkatesh, G., Deb, A., Karmarkar, A., and Chauhan, S.S. (2012) Effect of nanoclay content and compatibilizer on viscoelastic properties of montmorillonite/polypropylene nanocomposites. *Materials & Design*, **37**, 285–291.
- Verghese, K., Crossin, E., and Jollands, M. (2012) Packaging materials. Pp. 211 in: *Packaging for Sustainability* (K. Verghese, H. Lewis, L. Fitzpatrick, editors). Springer, California, USA.
- Villarroel, M., Fahl, N., De Sousa, A.M., and de Oliveira, O.B. (2011) Direct esthetic restorations based on translucency and opacity of composite resins. *Journal of Esthetic and Restorative Dentistry*, **23**, 73–87.
- Vyas, A. and Iroh, J.O. (2014) Thermal behavior and structure of clay/nylon-6 nanocomposite synthesized by *in situ* solution polymerization. *Journal of Thermal Analysis and Calorimetry*, **117**, 39–52.
- Wang, J.C., Xu, C., Hu, H., Wan, L., Chen, R., Zheng, H., Liu, F., Zhang, M., Shang, X., and Wang, X. (2011) Synthesis, mechanical, and barrier properties of LDPE/graphene nanocomposites using vinyl triethoxysilane as a coupling agent. *Journal of Nanoparticle Research*, **13**, 869–878.
- Wunderlich, B. and Czornyj, G. (1977) A study of equilibrium melting of polyethylene. *Macromolecules*, **10**, 906–913.
- Zanetti, M., Lomakin, S., and Camino, G. (2000) Polymer layered silicate nanocomposites. *Macromolecular Materials and Engineering*, **279**, 1–9.
- Zazoum, B., David, E., and Ngô, A. (2013) LDPE/HDPE/clay nanocomposites: Effects of compatibilizer on the structure and dielectric response. *Journal of Nanotechnology*, **2013**, 138457.
- Zazoum, B., David, E., and Ngô, A.D. (2014) Structural and dielectric studies of LLDPE/O-MMT nanocomposites. *Transactions on Electrical and Electronic Materials*, **15**, 235–240.
- Zbik, M.S. and Frost, R.L. (2010) Influence of smectite suspension structure on sheet orientation in dry sediments: XRD and AFM applications. *Journal of Colloid and Interface Science*, **346**, 311–316.
- Zhong, Y., Janes, D., Zheng, Y., Hetzer, M., and De Kee, D. (2007) Mechanical and oxygen barrier properties of organoclay-polyethylene nanocomposite films. *Polymer Engineering and Science*, **47**, 1101–1107.

(Received 18 August 2017; revised 19 October 2017; Ms. 1197; AE: H. Dong)